Remote sensing inversion of vegetation parameters with IPROSAIL-Net

Yunli Han, Yingying Dong, Yining Zhu, *Member*, *IEEE*, and Wenjiang Huang

***Abstract*—Vegetation parameters are important for the global carbon cycle. Therefore, the quantitative acquisition of vegetation parameters is crucial. The inverse process of the PROSAIL model has provided a classic method for vegetation parameter estimation. The current PROSAIL inverse process simulation, based on look-up tables and other methods, has challenges such as low accuracy and poor spatial universality. To address these issues, this study proposed a PROSAIL inverse process simulation method based on deep learning. The PROSAIL model was decomposed according to the physical process of the model. Then, the corresponding network module was designed based on the inverse process of each module and combined into the IPROSAIL-Net. This network uses the reflectance of the vegetation canopies as the input and presents the leaf structure parameter, chlorophyll a+b content Cab, equivalent water thickness, dry matter content Cm, and leaf area index (LAI) as the output. This article conducted experiments using two different sets of data. PROSAIL simulation data were used to invert the five values. The inversion accuracy was above 0.99 when the number of training samples reached more than 30,000. EnMAP data were used to invert the Cab and LAI values. When the number of training samples reached more than 120, the cereals accuracy was above 0.97 and the maize and rapeseed accuracies were above 0.99. The IPROSAIL-Net design was further split into six networks for separate trainings to verify its rationality. Therefore, the IPROSAIL-Net neural network is reasonable and feasible for remote sensing inversion of vegetation parameters.**

***Index Terms*—Convolutional neural network, EnMAP, Hyperspectral remote sensing, IPROSAIL-Net, PROSAIL model, Vegetation parameters**

I. INTRODUCTION

VEGETATION parameters are important indicators of vegetation's growth status. Quantitative acquisition of vegetation parameters is vital for precise agricultural research and is of great significance in supporting research on the carbon cycle [10, 19, 36]. Space-based remote sensing technology is an effective tool for extracting vegetation parameters [35]. At present, the main methods for remote sensing inversion of vegetation parameters include statistical methods and physically based model inversion methods [34]. Such statistical methods [11, 17, 23, 24] establish quantitative relationships between reflectance and vegetation parameters. Generally, the accuracy of these methods is higher than that of physically based model inversion methods, but they have geographic limitations and cannot explain causal relationships. Kennedy et al. [17] used parametric linear regression based on the vegetation index (VI), a nonparametric machine learning Gaussian regression equation (GPR), and inversion of the PROSAIL model using a look-up table approach (LUT) to invert the leaf and canopy biochemical and biophysical properties of Arctic vegetation. The experiment showed that the GPR, VI, and LUT methods had the highest, second highest, and lowest accuracies, respectively. Physically based model inversion methods [13, 21, 25] are based on the radiation transmission mechanism and have strong universal applicability. However, owing to the complexity of the model and the numerous model parameters, their accuracy and stability are limited. Current leaf and canopy parameter inversion methods based on physically based model inversion methods include LUT methods, optimisation methods, and neural network methods. The LUT method [1, 2, 16] has low parameter inversion accuracy due to the existence of "same-spectrum foreign objects." Abdelbaki et al. [1] introduced a new method to regularise the LUT method, which alleviated the problems of model uncertainty and measurement sensitivity, thereby improving inversion accuracy. Jiří et al. [16] used a combination of artificial neural networks and LUTs to retrieve the crop leaf area index (LAI), leaf chlorophyll content, and leaf water content. Among these methods, the LAI and leaf chlorophyll content parameters exhibited the best inversion results, whereas the water content parameter inversion results were unsatisfactory. The optimisation method [7, 20, 27] relies on the cost function and its initial value setting, which could lead to relatively large differences between the calculation time and convergence speed. Shanqin et al. [27] used the hyperparameter search algorithm tree-structure Parzen estimator to perform PROSAIL model inversion. The results were more accurate; however, prior knowledge of some of the PROSAIL model parameters was necessary. Sihem et al. [7] used the Bayesian method to conduct an inversion as a

This work was supported by National Key R&D Program of China (2021YFB3901303), Alliance of International Science Organizations (ANSO-CR-KP-2021-06), National Natural Science Foundation of China (42071423), National Natural Science Foundation of China (42071320), and SINO-EU, Dragon 5 proposal: Application Of Sino-Eu Optical Data Into Agronomic Models To Predict Crop Performance And To Monitor And Forecast Crop Pests And Diseases "ID 57457". (*Corresponding author: Yingying Dong*)

Y.L Han is with the State Key Laboratory of Remote Sensing Science, Aerospace Information Research Institute, Chinese Academy of Sciences, Beijing 100094, China (e-mail: hanyunli6688@163.com).

Y.Y. Dong and W. J. Huang are with the State Key Laboratory of Remote Sensing Science, Aerospace Information Research Institute, Chinese Academy of Sciences, Beijing 100094, China, and the University of Chinese Academy of Sciences, Beijing 100049, China (e-mail: dongyy@aircas.ac.cn; huangwj@aircas.ac.cn).

Y.N. Zhu is with the School of Mathematical Sciences, Capital Normal University, Beijing 100048, China (e-mail: ynzhu@cnu.edu.cn).

minimum cost function to solve the inversion problem. In comparison, the chlorophyll a+b content C_{ab} inversion results were superior.

Currently, deep learning applications [18, 26, 37, 39] are common. The development of methods for combining deep learning with a mechanism model has become a popular topic of research. A neural network can determine the internal connection between the input and output through learning and training based on the provided sample data. Therefore, a neural network can be used for nonlinear parameter inversion. Xu et al. [38] inverted rice canopy chlorophyll content and LAI based on radiative transfer and a Bayesian network model. The inversion accuracy was high, and maladaptation was effectively alleviated. Bahrami et al. [3] used four machine learning algorithms, namely support vector regression, random forest, gradient boosting (GB), and extreme gradient boosting (XGB) to estimate biophysical parameters. Experiments have shown that, of these algorithms, the GB and XGB algorithms show the best potential for crop parameter inversion.

This study combined the PROSAIL model with a neural network to construct a deep neural network coupled with a remote-sensing radiation transmission mechanism for the remote-sensing inversion of vegetation parameters. As the PROSAIL model is a nonlinear process, its inverse process cannot be resolved. The PROSAIL model was first decomposed into modules, and the network module was designed according to its physical processes. Stringing physically based modules into a network could fundamentally solve the lack of physical mechanisms in the inverse process of the PROSAIL model and improve the mechanism of the network. The inverse process of the PROSAIL model may simultaneously achieve the inversion of five leaf parameters, including the leaf structure parameter N, chlorophyll a+b content C_{ab}, equivalent water thickness C_w, dry matter content C_m, and the LAI.

II. Method

2.1. Modularisation of the PROSAIL model

The PROSAIL model [5, 15] is a radiation transfer model based on mathematics, physics, and ecology. The principle on which this model is based makes it one of the most popular radiative transfer tools, and it plays an important role in the quantitative inversion of leaf and canopy parameters. The PROSAIL model uses leaf reflectance and transmittance obtained from the leaf optical characteristic model (PROSPECT) as parameters and inputs them into the canopy bidirectional reflectance model (SAIL) to obtain the vegetation canopy reflectance. We first split the PROSAIL model into PROSPECT and SAIL models and then further divided the two models to obtain various small modules. These modules were integrated to form a modular decomposition of the PROSAIL model.

2.1.1. Modularisation of the PROSPECT model

The PROSPECT model [4, 6, 8, 9, 12, 14] is a radiative transfer model based on Allen's generalised "plate model" The model uses two types of parameters: leaf structure parameter N and leaf biochemical parameters C_{ab}, C_w, C_m, brown pigment content C_{brown}, and carotenoid C_{ar}. Model inversion allows the reconstruction of the leaf reflectance and transmittance features in the 400-2500 nm range by adjusting six input parameters.

The PROSPECT model first solves the leaf transmission coefficient based on the optical characteristics of the plant leaves. It then uses the "plate model" to solve the leaf reflectance and transmittance for one leaf structure. Stokes' theory is used to solve the leaf reflectance and transmittance when there is more than one leaf structure. Therefore, we divided the PROSPECT model into the following three modules.

Module 1: Solve the transmission coefficient of the plate θ, which is a nonlinear function of all the input parameters. The formula is:

$$\theta=(1-k)e^{-k}+k^2\int_k^{\infty}N^{-1}e^{-k}dx \tag{1}$$

$$k(\lambda)=\sum K_i(\lambda)C_i \tag{2}$$

where λ is the wavelength, $K_i(\lambda)$ is the spectral specific absorption coefficient relative to leaf component I, and C_i is the leaf component i content per unit of leaf area.

Module 2: Solve leaf reflectance ρ_α and transmittance τ_α, where N is equal to 1, and ρ_α and τ_α are nonlinear functions of θ. The formula is:

$$\rho_\alpha=\left[1-t_{\alpha v}(\alpha,n)\right]+\frac{t_{\alpha v}(90,n)t_{\alpha v}(\alpha,n)\theta^2\left[n^2-t_{\alpha v}(90,n)\right]}{n^4-\theta^2\left[n^2-t_{\alpha v}(90,n)\right]^2} \tag{3}$$

$$\tau_\alpha=\frac{t_{\alpha v}(90,n)t_{\alpha v}(\alpha,n)\theta^2n^2}{n^4-\theta^2\left[n^2-t_{\alpha v}(90,n)\right]^2} \tag{4}$$

where α is the maximum incidence angle defining the solid angle, n is the refractive index, and $t_{\alpha v}(\alpha,n)$ is the transmissivity of the dielectric plane surface averaged over all incidence directions and polarisations.

Module 3: Solve leaf reflectance $R_{N,\alpha}$ and transmittance $T_{N,\alpha}$, where N is not equal to 1, and $R_{N,\alpha}$ and $T_{N,\alpha}$ are both nonlinear functions of ρ_α and τ_α. The formula is:

$$R_{N,\alpha}=\rho_\alpha+\frac{\tau_\alpha\tau_{90}R_{N-1,90}}{1-\rho_{90}R_{N-1,90}} \tag{5}$$

$$T_{N,\alpha}=\frac{\tau_\alpha T_{N-1,90}}{1-\rho_{90}R_{N-1,90}} \tag{6}$$

Based on the principle of the PROSPECT model and the relationship between the three modules, connecting several modules in series forms a modular decomposition of the PROSPECT model (Fig.1).

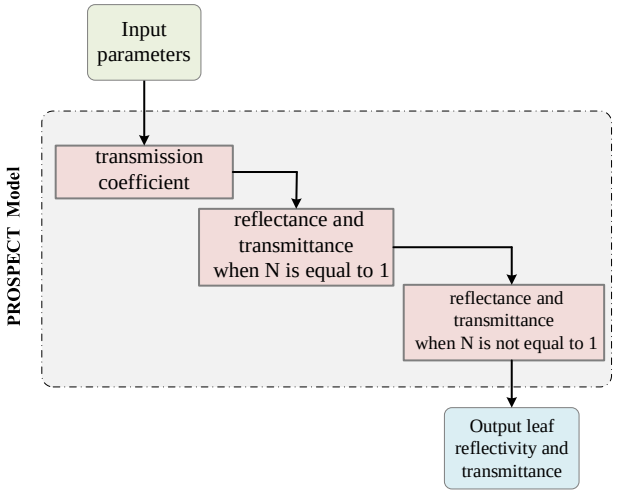


Fig. 1. Module decomposition of the PROSPECT model

2.1.2. Modularisation of the SAIL model

The SAIL model [29, 30, 31, 32, 33] is an improved version model of the Suits model. It simulates the bidirectional reflectance factor of turbid medium plant canopies by solving for scattering and absorption of four upward/downward radiative fluxes. The model parameters were divided into four categories: leaf parameters (LAI, leaf inclination distribution functions [LIDFa and LIDFb], and leaf angle distribution type [TypeLidf]), soil parameters (soil reflectance [Psoil]), hot spot parameters (hspot), and angle parameters (solar zenith angle [tts], viewing zenith angle [tto], and relative azimuth angle [psi]).

The SAIL model mainly describes the relationship between the luminous fluxes of different categories and directions between the leaf layers, vegetation parameters, and the transmittance and reflectivity of the vegetation canopy. These are characterised as:

$$\begin{aligned}
\frac{dE_s}{Ldx} &= kE_s \\
\frac{dE^-}{Ldx} &= -s'E_s + aE^- - \sigma E^+ \\
\frac{dE^+}{Ldx} &= -sE_s + \sigma E^- - aE^+ \\
\frac{dE_o}{Ldx} &= wE_s + vE^- + v'E^+ - KE_o
\end{aligned} \tag{7}$$

where L is the *LAI*, and x is the thickness of the layer which was set to 0 for the top of the layer and -1 for the bottom of the layer. Coefficients k, s', a, σ, w, v, v', and K are the extinction and scattering coefficients that describe the interactions between the four flux types.

The general solution of this system of differential equations is:

$$\begin{aligned}
&E_s(-1) = \tau_{ss}E_s(0) \\
&E^-(-1) = \tau_{sd}E_s(0) + \tau_{dd}E^-(0) + \rho_{dd}E^+(-1) + \gamma_d H_v \\
&E^+(0) = \rho_{sd}E_s(0) + \rho_{dd}E^-(0) + \tau_{dd}E^+(-1) + \gamma_d H_v \\
&E_o(0) = \rho_{so}E_s(0) + \rho_{do}E^-(0) + \tau_{do}E^+(-1) + \tau_{oo}E_o(-1) + \gamma_0 H_v = r_{so}E_s(0) + r_{do}E^-(0)
\end{aligned} \tag{8}$$

Based on its formula and process, the SAIL model is divided into the following six modules:

Module 1: Calculating extinction and scattering coefficients. These values are calculated from the input parameters of the SAIL model.

Module 2: Solving ρ_{dd}, τ_{ss}, τ_{oo}, and τ_{dd}. The reflectivity and transmittance of this part of the interaction are calculated directly from the extinction and scattering coefficients, which are expressed as

$$\begin{aligned}
\rho_{dd} &= (e^m - e^{-m}) / (h_1 e^m - h_2 e^{-m}) \\
\tau_{ss} &= e^{-k} \\
\tau_{oo} &= e^{-K} \\
\tau_{dd} &= (h_1 - h_2) / (h_1 e^m - h_2 e^{-m}) \\
m &= \sqrt{a^2 - \sigma^2} \\
h_1 &= \frac{1}{h_2} = (a+m)/\sigma
\end{aligned} \tag{9}$$

where ρ_{dd} represents the diffuse reflectance for diffuse incidence of a layer, τ_{ss} represents the direct transmittance in the direction of the sun, τ_{oo} represents the direct transmittance in the direction of observation, and τ_{dd} represents the diffuse transmittance for diffuse incidence.

Module 3: Solving ρ_{sd} the ρ_{do}, τ_{sd}, τ_{do}, and ρ_{so}^d. When solving the SAIL model, the denominator may be zero, namely, the singularity problem. The data calculation method for this problem is provided in the 4SAIL model [33]. These parameters are calculated using the model.

Module 4: Solving τ_{ssoo} and ρ_{so}^s. When a hotspot effect occurs, a correction needs to be made to the SAIL and SAILH models [31], according to which the above parameters can be calculated.

Module 5: Solving r_{so} and r_{do}, where r_{so} is affected by the hot spot effect. Both values are also affected by singularity.

$$\begin{aligned}
r_{so} &= \rho_{so} + \left[\tau_{ssoo} + \frac{(\tau_{sd} + \tau_{ss} r_s \rho_{dd})\tau_{oo} + (\tau_{ss} + \tau_{sd})\tau_{do}}{1 - r_s \rho_{dd}} \right] r_s \\
r_{do} &= \rho_{do} + \frac{\tau_{dd} r_s (\tau_{oo} + \tau_{do})}{1 - r_s \rho_{dd}}
\end{aligned} \tag{10}$$

Module 6: Solving the vegetation canopy reflectance R, which is a function of r_{so} and r_{do}:

$$\begin{aligned}
R &= \frac{E_o}{E_{sun} + E_{sky}} \\
&= r_{so}(1 - SKYL) + r_{do} SKYL
\end{aligned} \tag{11}$$

$$SKYL = \frac{E_{sky}}{E_{sun} + E_{sky}} \tag{12}$$

where E_{sun} and E_{sky} are direct sunlight and diffuse skylight, respectively, when $x = 0$.

According to the mechanism of the SAIL model and the relationship between the six modules, the modular decomposition of the SAIL model is formed by connecting several modules in series (Fig.2).

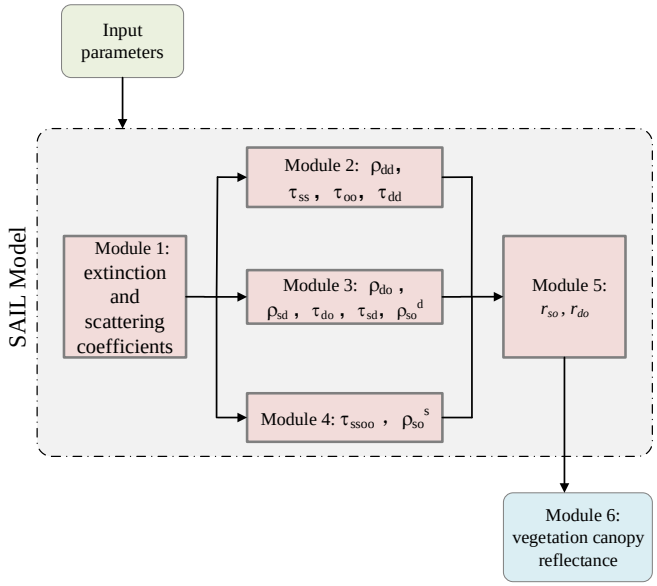


Fig. 2. Module decomposition of the SAIL model

2.2. Vegetation parameters inversion with IPROSAIL-Net

2.2.1. Basic structure of the neural network

Convolutional neural networks are widely used to prevent spatial information loss, as they have fewer parameters, perform fast feature training, and prevent overfitting. The main structure of convolutional neural networks includes an input layer, convolutional layer, activation layer, pooling layer, and fully connected layer.

The convolutional layer is the core layer of the convolutional network, and the main functions of the convolutional layer are to extract the spatial characteristics of the hyperspectral image through the mechanism of local perception and "weight sharing" in order to reduce the number of parameters.

The formula is:

$$S(i,j)=(I*K)(i,j)=\sum_{m}\sum_{n}I(i+m,j+n)K(m,n) \quad (13)$$

where I is the hyperspectral image and K is the convolution kernel.

The pooling layer generally follows a convolutional layer and its essence is sampling. Common pooling layer operations include maximum, average, and random pooling. The maximum pooling operation was selected in this study, The purpose of the pooling layer is to reduce the number of network parameters, impute the scale invariance and rotation invariance of the spectral image, and prevent overfitting.

The fully connected layer mainly maps the spectral image characteristics to the leaf parameters, playing the role of the "classifier." The formula is:

$$Z_h = Y_{h-1} * W_h + B_h \quad (14)$$

where h is the hth layer, W_h is the weight of the hth layer, B_h is the hth-layer bias term, and Y_{h-1} is the output of the hth layer.

The activation layer primarily improves the nonlinear expression ability of the network. In this study, a ReLU activation function was selected.

2.2.2. IPROSAIL-Net convolutional neural network design and inversion process

To improve the neural network mechanism and accuracy of vegetation parameter inversion, the PROSAIL model was first decomposed into modules according to the physical process. Then, the network modules were designed for solving each module, and were finally combined into an end-to-end IPROSAIL-Net for parameter inversion (Fig.3). IPROSAIL-Net transfers 1×244 spectrum data into a network that replaces the inverse process of the SAIL model to obtain leaf reflectance and transmittance. These values are then transferred to a network that replaces the inverse processes of the PROSPECT model. Leaf parameters N, C_{ab}, C_w, and C_m were thus obtained. Because LAI is a parameter of the SAIL model, LAI was obtained by inverting the network branch of the inverse process in the SAIL model. The 1×244 spectrum data is a simulation of the EnMAP data with a spectral range of 420-2460nm and 244 bands.

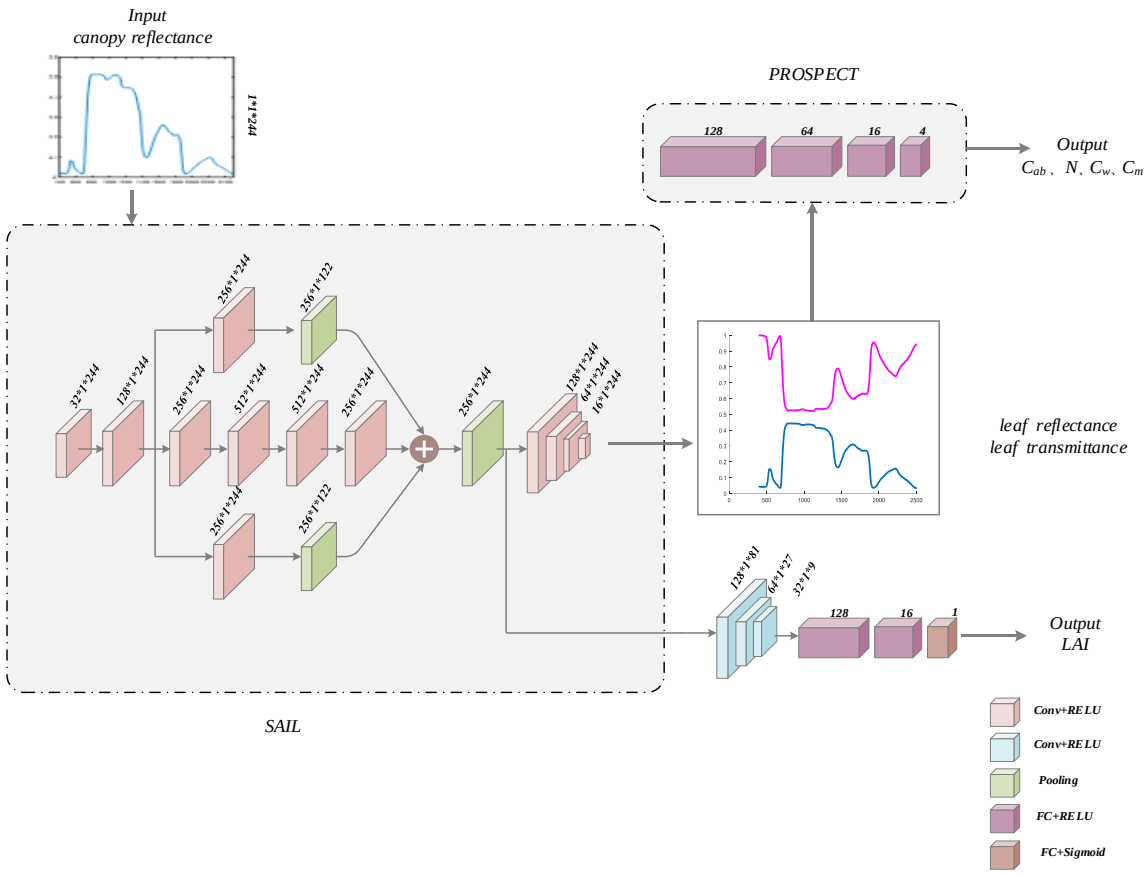


Fig. 3. IPROSAIL-Net neural network structure

Based on the physical process of the PROSAIL model, we first replaced the inverse process of the SAIL model module to solve the network. The first module of the SAIL model's inverse process involves solving for the vegetation canopy reflectance *R*. Instead, this module chose a convolutional layer, where the size of the convolution kernel was 1×3, the padding was $(0,1)$, and the number of channels was 32. Because this module was a nonlinear process, the ReLU activation function was added to increase its nonlinear expression ability. This step mainly extracted the main characteristics of the spectrum and the local connection of the convolution, where the "parameter sharing" feature greatly reduced the network parameters, ensured the sparsity of the network, and prevented overfitting. Through this process, $32\times 1\times 244$ spectral features were obtained.

The second module of the inverse process of the SAIL model involves solving r_{so} and r_{do}. This module selects a convolutional layer where the size of the convolution kernel was 1×3, padding was $(0,1)$, and the number of channels was 128. The ReLU activation function was added. Through this process, $128\times 1\times 244$ spectral features were obtained.

The third module of the inverse process of the SAIL model involves solving τ_{ssoo} and ρ_{so}^{s}. As this module has many formulas and strong nonlinearity, four convolutional layers were used, and a ReLU activation function was added to each layer to increase its nonlinear expression ability. The size of the convolution kernel of each layer was 1×3, the padding was $(0,1)$, and the numbers of channels were 256, 512, 521, and 256. In this step, more spectral feature types were extracted by increasing the number of convolution kernels, and more spectral information was retained. Through this process, $256\times 1\times 244$ spectral features were obtained.

The fourth module of the inverse process of the SAIL model involves solving ρ_{sd}, ρ_{do}, τ_{sd}, τ_{do}, and ρ_{so}^{d}. This module used the convolutional and pooling layers. Because this was a nonlinear process, the ReLU activation function was added after the convolutional layer. The convolutional layer selected a convolution kernel size of 1×3, the padding was $(0,1)$, and the number of channels was 256. This process resulted in $256\times 1\times 244$ spectral features. The maximum pooling layer was then passed through with a pooling size of 1×2, and the $256\times 1\times 122$ spectral features were obtained. The purpose of adding a pooling layer was to extract the most important features and reduce the dimensionality of the spectrum to prevent overfitting.

The fifth module of the inverse process of the SAIL model involved solving ρ_{dd}, τ_{ss}, and τ_{oo}. This module chose the convolutional and pooling layers and added the ReLU activation function after the convolutional layer. To fully

express each spectrum, choosing an excessively large convolution kernel was not appropriate. Therefore, a convolution kernel size of 1×3 was used, and the padding was $(0,1)$. For the splicing operation, the number of convolution kernel channels was set to 256. The maximum pooling layer selected the pooling size using 1×2. The results show the $256\times1\times122$ spectral features.

Based on the decomposition principle of the SAIL model modules, the spectral features were first obtained from the third, fourth, and fifth modules, and then spliced to obtain the $256\times1\times488$ spectral features. The maximum pooling layer was then passed through with a pooling size of 1×2. The results showed the $256\times1\times244$ spectral features.

The sixth module of the inverse process of the SAIL model included the inverse process for solving the extinction and scattering coefficients. Owing to the complexity of this process, four convolutional layers were selected and the ReLU activation function was added to each layer. The size of the convolution kernel of each layer was 1×3, the padding was $(0,1)$, and the numbers of channels were 128, 64, 16, and 2. This process achieved $2\times1\times244$ spectral features representing the reflectance and transmittance of the leaves.

The seventh module of the SAIL model involved an inverse process for solving the *LAI*. This process was derived from the reverse process network of the SAIL model. This process was parallel to the sixth module of the inverse process based on the decomposition principle of the SAIL model modules. Its input included the $256\times1\times244$ spectral features. This module selected four convolutional layers and three fully connected layers. A ReLU activation function was added to each layer to increase the nonlinear expression capability, except for the last layer, in which the Sigmoid activation function was added. The size of the convolution kernel of each layer was 1×3, the stride was $(1,3)$, and the numbers of channels were 128, 64, and 32. The numbers of neurons were 128, 16, and 1, respectively. The *LAI* values were then obtained from these values.

Subsequently, the inverse process of the PROSPECT model was performed. Its inputs included the leaf reflectance and transmittance obtained from the inverse process of the SAIL model. The calculation of the PROSPECT model was nonlinear. The inverse process of the PROSPECT model was replaced by four fully connected layers. The numbers of neurons were 128, 64, 16, and 4. The ReLU activation function was added to replace the nonlinear process after each layer. This process mapped the image characteristics of the reflectance and transmittance of the leaf-to-leaf parameters. Four leaf parameters were obtained: N, C_{ab}, C_w, and C_m.

2.2.3. Training and verification of the convolutional neural network

Network training minimises the loss function through forward and backward propagations (Fig. 4). As IPROSAIL-Net is a regression problem network, the mean square error loss function was selected to estimate the error, as shown in Eq. (15). The Adam algorithm was used as the optimisation method, which continuously updates the parameters through positive and negative processes for the loss function to reach the global minimum.

$$MSE\left(y,y^{'}\right)=\frac{1}{n}\sum_{i=1}^{n}\left(y_i-y_i^{'}\right)^2 \tag{15}$$

where y_i is the i-th label value of the leaf parameter, $y_i^{'}$ is the predicted value of the network, and n is the number of leaf parameters to be solved, which is equal to five.

First, simulated data were preprocessed. A number of samples were randomly selected for training, verification, and testing. Three sample groups were obtained once with proportions of 60%, 20%, and 20%. Including the input value, spectral reflectance, and its corresponding label value, N, C_{ab}, C_w, C_m, and LAI were used to facilitate convergence. Five vegetation parameter values were normalised.

After initialising the weights, the spectral reflectance of the training and verification samples were transferred to the network in batches. The leaf parameters were calculated using IPROSAIL-Net, as shown in Eqs. (16). The loss function was then used to find the sum tag value error, thus completing the forward propagation.

$$y=\sigma(xW+b) \tag{16}$$

where y is the output vegetation parameter, which is a five-dimensional vector; x is the number of input spectral reflectance; W and b are the weights and bias terms of the convolutional and fully connected layers, respectively; $\sigma(x)$ is the activation function.

The next step included backward propagation using the Adam algorithm for the gradient descent. Default parameters were selected using the PyTorch framework. The network hyperparameters were set to the data batch size $batchsize=100$, iteration number $epoch=2000$, and initial learning rate lr=0.001. Because the learning rate was prohibitively high, which may cause the model to miss the optimal solution, the learning rate decay speed was set to 500 times per iteration ($lr=lr\times0.8$). As this was a batch of input data, the mean cost function of the mean-squared error (MSE) was used, as shown in Eq. (18). The Adam algorithm was applied to calculate the gradient of each function and update its weight. The updated weight formulae are given by Eqs. (17) and (19) as follows:

$$J(y,y^{'})=\frac{1}{batchsize}\sum_{i=1}^{batchsize}MSE(y,y^{'}) \tag{17}$$

$$W=W-lr\frac{\partial J(W,b)}{\partial W} \tag{18}$$

$$b=b-lr\frac{\partial J(W,b)}{\partial b} \tag{19}$$

Forward and backward propagations were performed using this method. The network parameters were updated through forward and backward propagation. Each iteration was updated to complete an *epoch*. Through continuous iterations, the cost

function was continuously reduced. Finally, convergence was achieved.

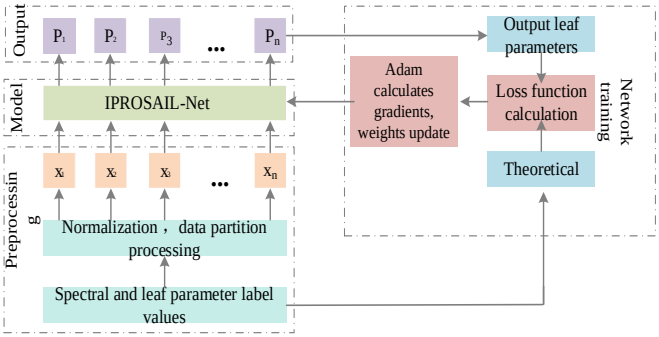


Fig. 4. IPROSAIL-Net training process

The network was verified by taking the simulated values of the vegetation parameters *N*, C_{ab}, C_w, C_m, and *LAI* in the trained network from the input of the test set. R^2 and root mean square error (*RMSE*) of the real values were calculated using these two values and the image to characterise the results of the inversion.

III. Experiments Results and Analysis

3.1. Quantitative inversion of the vegetation parameters based on PROSAIL simulation data

3.1.1. Data simulation

This study assessed simulated data to verify the effects of the network. The PROSAIL model was used to fix the seven model parameters. The remaining eight parameters utilised values within a certain range, as listed in TABLE I. The method involved selecting $0 \sim 1$ random number *rand*, using Eq. (20) to obtain the random values of these eight parameters and then randomly combining their values. A total of 500,000 loops were used to obtain 500,000 values in the range of 400-2500 nm. The spectral data were stripped and the spectral response function in Eq. (21) was used to divide the spectrum into 244 bands.

$$x = x_{\min} + rand\left(x_{\max} - x_{\min}\right) \tag{20}$$

$$R = \frac{\sum_{i=b_{start}}^{b_{end}} f\left(x_i\right) R_{PHIi}}{\sum_{i=b_{start}}^{b_{end}} f\left(x_i\right)} \tag{21}$$

where *R* represents the reflectance of the simulated data and b_{start} and b_{end} represent the start and end wavelengths of the spectrum, respectively. In our study, b_{start} = 400 nm, b_{end} = 2500 nm, and $f\left(x_i\right)$ were the values of the spectral response function in the *i*-th band, and R_{PHIi} was the reflectance.

TABLE I
PROSAIL MODEL PARAMETERS

Model	Parameter	Range	Unit
PROSPECT	N	1.0~2.5	-
	C_{ab}	5~90	$\mu g \cdot cm^{-2}$
	C_w	0.001~0.05	cm
	C_m	0.001~0.03	$g \cdot cm^{-2}$
	C_{ar}	10	$\mu g \cdot cm^{-2}$
	C_{brown}	0	-
SAIL	LAI	0~10	-
	$LIDFa$	30~80	deg
	$LIDFb$	0	-
	$TypeLidf$	2	-
	$hspot$	0.01~1	-
	p_{soil}	0~1	-
	tts	30	deg
	tto	10	deg
	psi	10	deg

3.1.2. Quantitative inversion of vegetation parameters based on IPROSAIL-Net with PROSAIL simulation data

A numerical experiment of the IPROSAIL-Net inversion of vegetation parameters was performed using PROSAIL simulation data as the experimental data. To test the dependence of IPROSAIL-Net on the data, the number of training samples was set to 300,000, 60,000, 30,000, 6,000, 3,000, and 1,500. The training samples and corresponding number of verification samples were then sent to the model training network. The test samples were transferred to the trained network, and vegetation parameters were obtained by inversion. R^2 and the *RMSE* were calculated. the thermal scatter diagram is shown in Fig. 5, and the accuracy diagram is shown in Fig. 6.

The experimental results showed that the inversion accuracies of the five vegetation parameter values retrieved using IPROSAIL-Net were all greater than 0.94. When the training sample size was greater than 30,000, the inversion accuracies of all five vegetation parameter values were above 0.99. Large training samples were correlated with a larger R^2 for the five vegetation parameter values and a smaller *RMSE*. The predicted values were closer to the true values. We propose that IPROSAIL-Net is suitable for the high-precision inversion of vegetation parameters.

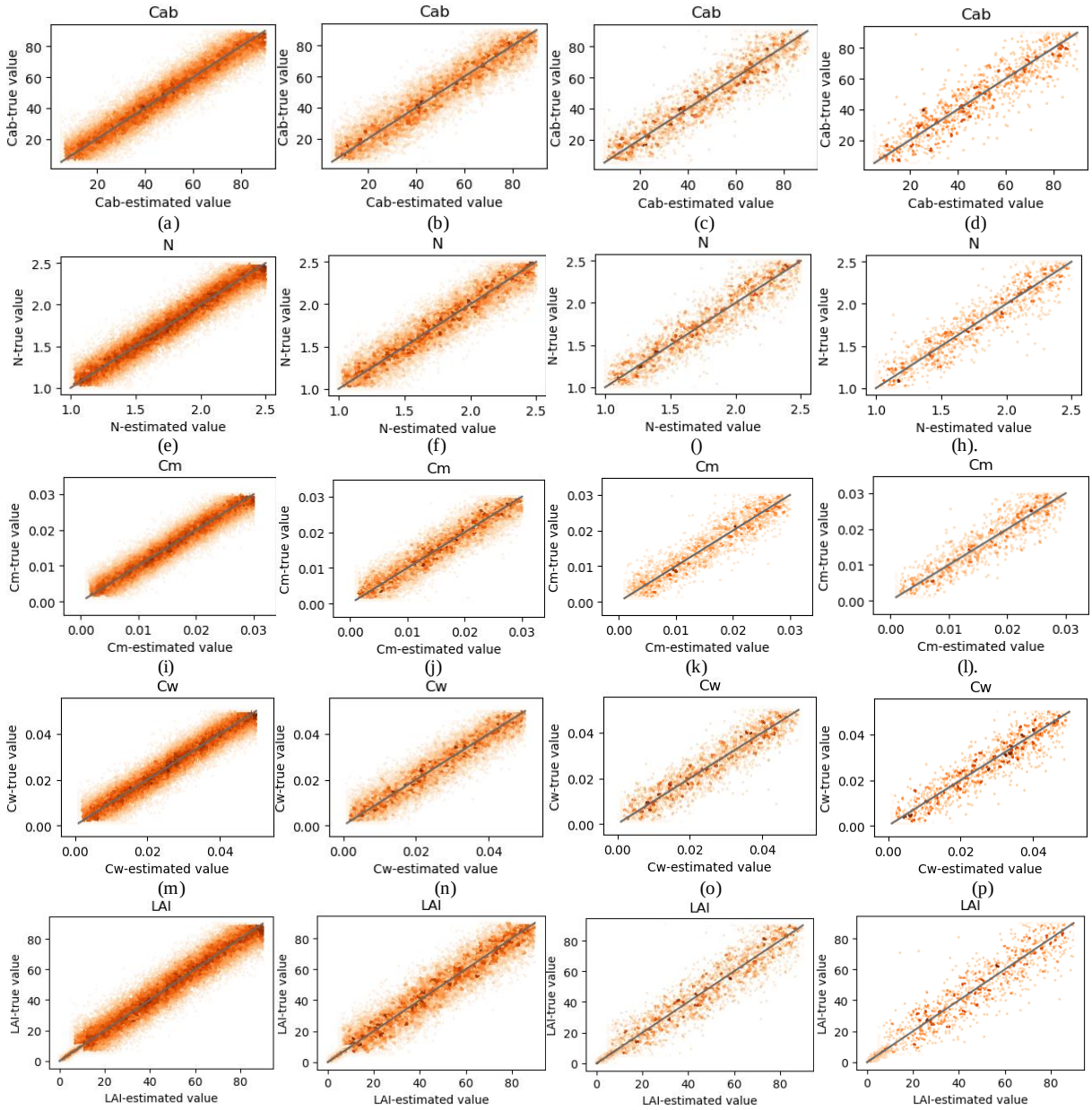
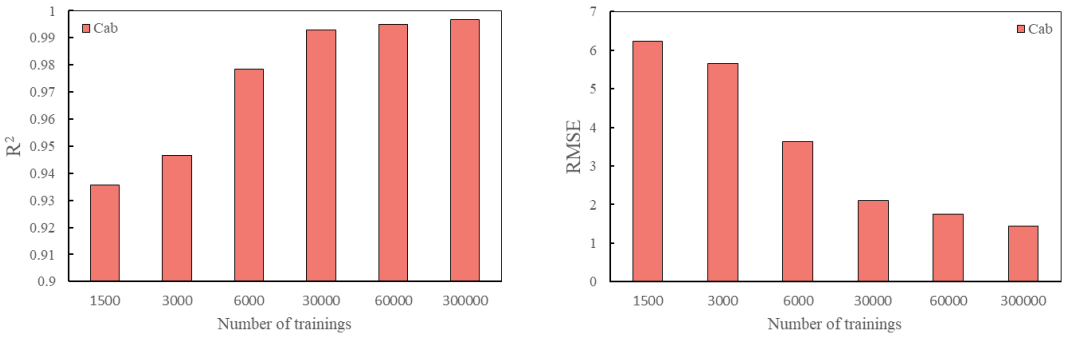


Fig.5. Thermal scatter plots of the vegetation parameters inversion with the IPROSAIL-Net. (a), (b), (c) and (d) are the scatter plots of chlorophyll a+b content (C_{ab},) under net_{300000}, net_{30000}, net_{6000}, and net_{3000}, respectively. (e), (g), (f) and (h) are the scatter plots of N under net_{300000}, net_{30000}, net_{6000}, and $net_{3000,}$ respectively. (i), (j), (k) and (l) are the scatter plots of dry matter content (C_m) under net_{300000}, net_{30000}, net_{6000}, and net_{3000}, respectively. (m), (n), (o) and (p) are the scatter plots of equivalent water thickness (C_w) under net_{300000}, net_{30000}, net_{6000}, and net_{3000}, respectively. (q), (r), (s) and (t) are the scatter plots of leaf area index (LAI) under net_{300000}, net_{30000}, net_{6000}, and net_{3000}, respectively.



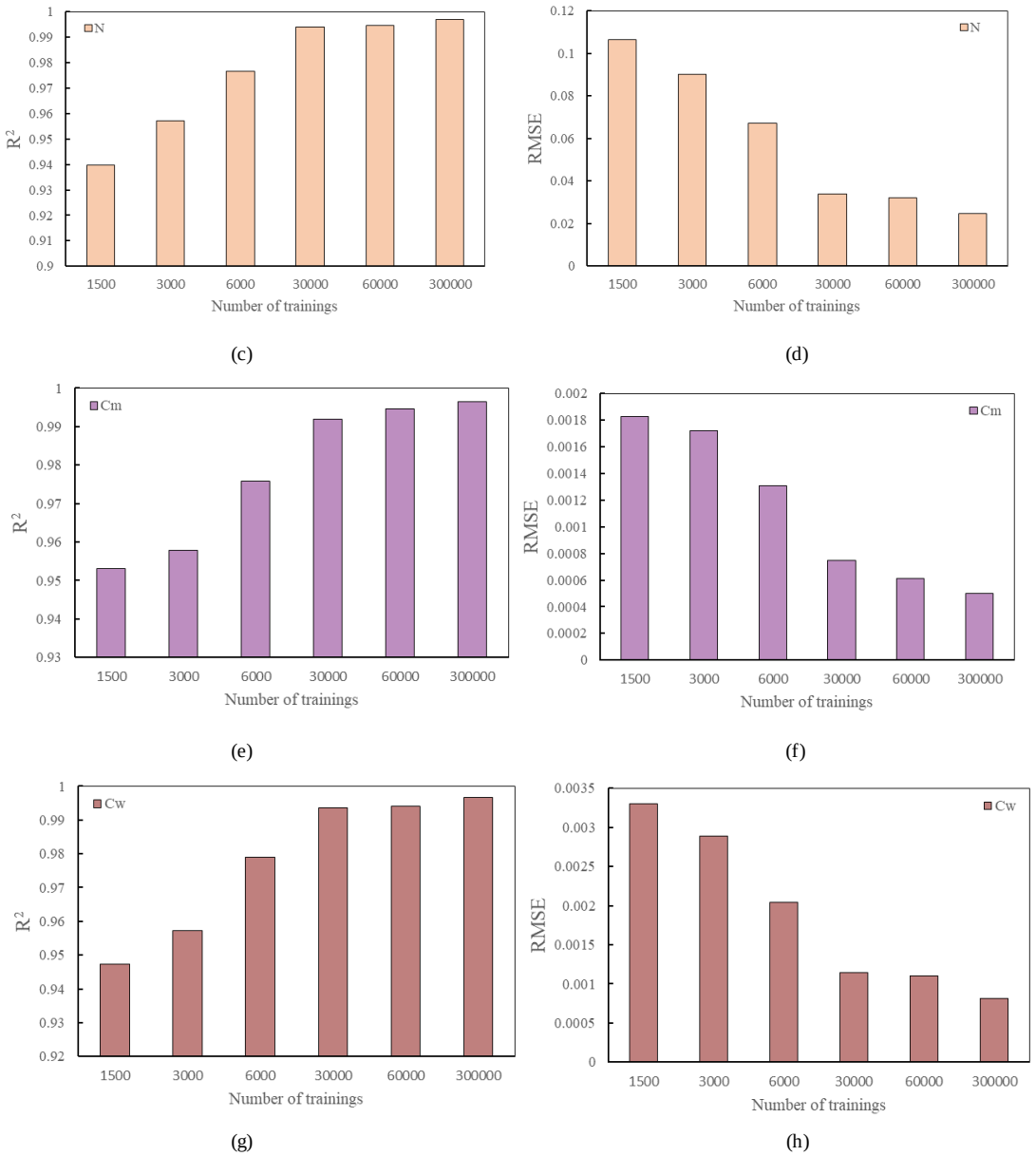


Fig. 6. Accuracy map of the vegetation parameters inversion based on IPROSAIL-Net with simulation data

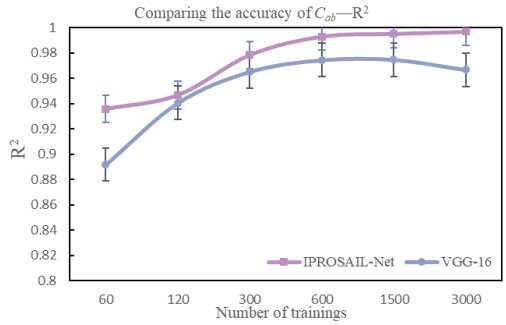
3.1.3. Quantitative inversion of vegetation parameters based on IPROSAIL-Net with PROSAIL simulation data

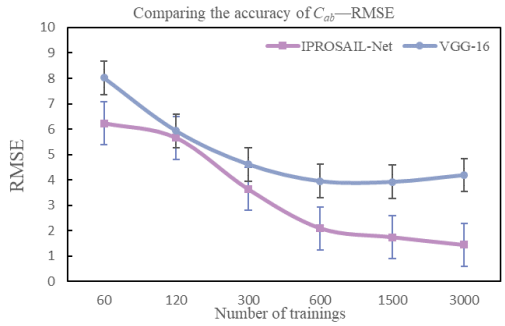
The classic deep convolutional neural network architecture of VGG (Visual Geometry Group) features simplicity and ease of implementation, which makes VGG networks widely used in computer vision tasks such as image classification, object detection, and semantic segmentation [28]. Therefore, the VGG-16 network was selected for vegetation parameter inversion in this comparative analysis. The convolution kernel size of the VGG-16 network was set to 1×3, the stride was $(1,1)$, and the padding was $(0,1)$. The maximum pooling layer size was 1×2, the stride was $(1,2)$, and the numbers of neurons in the fully connected layer were 128, 64, and 4. The sample selection and training methods for the VGG-16 and IPROSAIL-Net were identical. The vegetation parameter inversion results and comparisons are presented in TABLE II and Fig. 7.

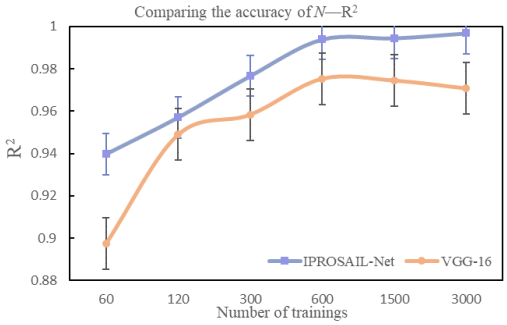
TABLE II
COMPARISON OF VEGETATION PARAMETER INVERSION RESULTS BASED ON THE IPROSAIL-NET AND VGG-16 NETWORKS WITH SIMULATED DATA

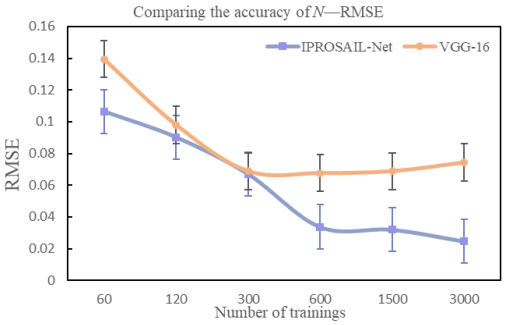
Model	Number of trainings	C_{ab}		N		C_m		C_w		LAI	
		R^2	RMSE	R^2	RMSE	R^2	RMSE	R^2	RMSE	R^2	RMSE

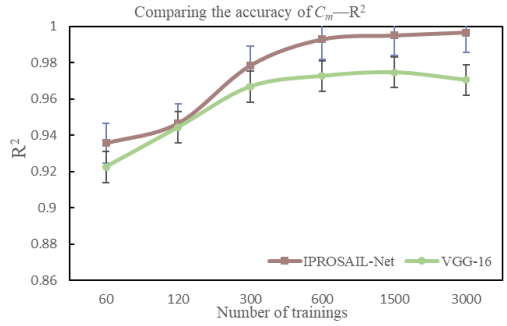
IPROSAIL-Net	300000	**0.99**	**1.44**	**0.99**	**0.02**	**0.99**	**0.0005**	**0.99**	**0.0008**	**0.99**	**0.17**
VGG-16		0.97	4.18	0.97	0.07	0.97	0.001	0.97	0.002	0.97	0.9
IPROSAIL-Net	60000	**0.99**	**1.74**	**0.99**	**0.03**	**0.99**	**0.0006**	**0.99**	**0.001**	**0.99**	**0.21**
VGG-16		0.97	3.91	0.97	0.06	0.97	0.001	0.97	0.002	0.97	0.40
IPROSAIL-Net	30000	**0.99**	**2.09**	**0.99**	**0.03**	**0.99**	**0.0008**	**0.99**	**0.001**	**0.99**	**0.23**
VGG-16		0.97	3.94	0.98	0.07	0.97	0.001	0.98	0.002	0.97	0.46
IPROSAIL-Net	6000	**0.98**	**3.64**	**0.98**	**0.07**	**0.98**	**0.001**	**0.98**	**0.002**	**0.97**	**0.37**
VGG-16		0.96	4.61	0.96	0.09	0.97	0.002	0.97	0.003	0.97	0.51
IPROSAIL-Net	3000	**0.95**	**5.67**	**0.95**	**0.09**	**0.96**	**0.002**	**0.96**	**0.003**	**0.95**	**0.58**
VGG-16		0.94	5.93	0.95	0.10	0.94	0.002	0.94	0.003	0.95	0.65
IPROSAIL-Net	1500	**0.94**	**6.23**	**0.94**	**0.11**	**0.95**	0.002	**0.95**	**0.003**	**0.92**	**0.81**
VGG-16		0.89	8.02	0.90	0.14	0.92	0.002	0.92	0.004	0.89	0.95

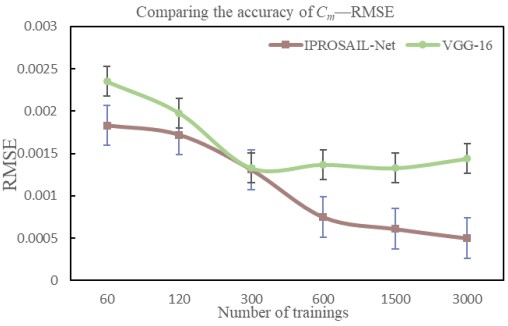












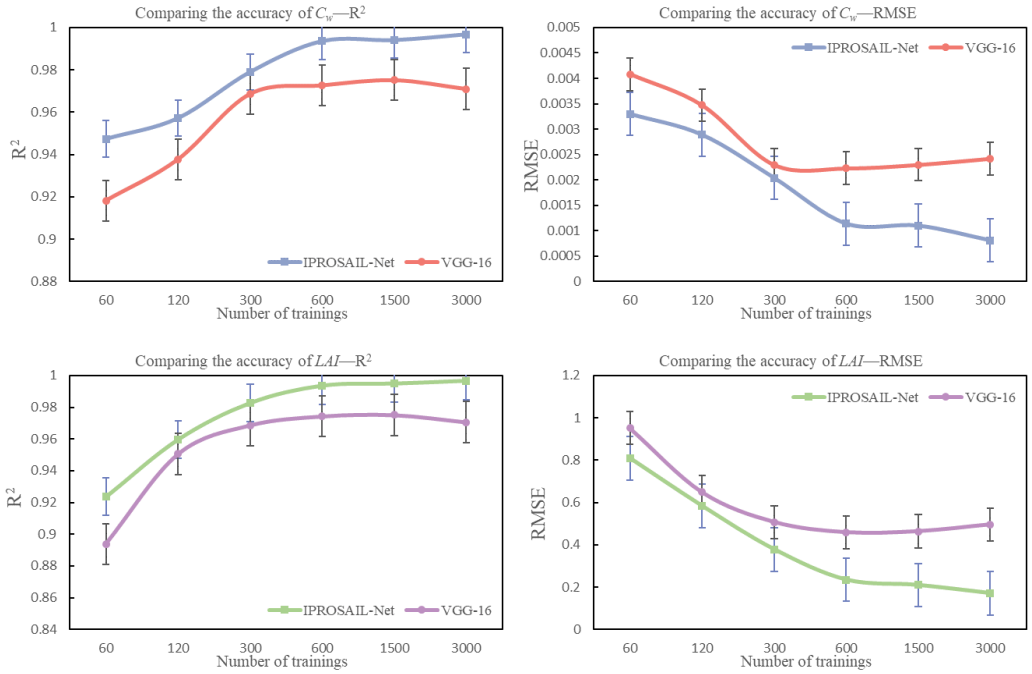


Fig. 7. Vegetation parameters accuracy comparison with PROSAIL simulation data

The results of the numerical experimental analysis showed that the inversion accuracy of IPROSAIL-Net was higher than that of the VGG-16 network and that the *RMSE* of IPROSAIL-Net was lower than that of the VGG-16 network. When the number of training samples was greater than 30,000, the accuracy of the inverted vegetation parameters of the VGG-16 network remained above 0.97, and the accuracy of IPROSAIL-Net was above 0.99. When the number of training samples was 300,000, the R^2 values of C_{ab}, N, C_m, C_w, and *LAI* obtained by the inversion of the VGG-16 network were 0.97, and the *RMSE* values were 4.18, 0.07, 0.001, 0.002, and 0.90, respectively. The R^2 values of C_{ab}, N, C_m, C_w, and *LAI* obtained by the IPROSAIL-Net inversion were all above 0.99, and the *RMSE* values were 1.44, 0.07, 0.005, 0.0008, and 0.17, respectively. In summary, the IPROSAIL-Net inversion of the vegetation parameters achieved satisfactory results.

IPROSAIL-Net is suitable for high-precision inversion of vegetation parameters. This is because the network was combined with the PROSAIL radiation transmission model to improve the mechanism of the neural network. The PROSAIL model is divided into modules. The principles of network construction and modules were used to replace the various modules of the inverse process and were finally combined into IPROSAIL-Net. The VGG-16 network determines the theoretical basis; therefore, its inversion accuracy is lower than that of IPROSAIL-Net. Consequently, IPROSAIL-Net is suitable for high-precision inversion of vegetation parameters.

3.2. Quantitative inversion of Cab and LAI with EnMAP data

3.2.1. Quantitative inversion of Cab and LAI based on IPROSAIL-Net with EnMAP data

To test the inversion of the vegetation parameters with the IPROSAIL-Net using different data sets, hyperspectral data of the EnMAP satellite located in the foothills of the German Alps (48. 0514 N, 11. 0760 E) were selected. This set of data was acquired on July 22, 2006, and included the hyperspectral reflectance and C_{ab} and *LAI* concentrations of cereals, maize, and rapeseed in the area. The hyperspectral reflectance was processed by the atmosphere and contained 244 bands. The distribution maps of the main crops, C_{ab} images, and *LAI* images are shown in Fig. 8.

Numerical experiments were performed using the C_{ab} and *LAI* vegetation concentrations in IPROSAIL-Net with EnMAP data. To test the dependence of IPROSAIL-Net on the data, the number of training samples was set to 6,000, 3,000, 1,500, 600, 300, 120, and 60. The C_{ab} and *LAI* concentrations were obtained by inversion. The R^2 and *RMSE* were calculated using true values. the accuracy results are shown in Fig. 9.

The experimental results showed that the accuracy of C_{ab} and *LAI* inversions based on the EnMAP data was greater than 0.91. The *RMSE* of C_{ab} and *LAI* were below 4.25 and 0.68, respectively. A large number of trainings correlated with a larger R^2 and smaller *RMSE*. The C_{ab} and *LAI* concentrations could, therefore, be inverted with high accuracy using EnMAP data, indicating that IPROSAIL-Net can invert vegetation parameters with high accuracy and support small data training samples.

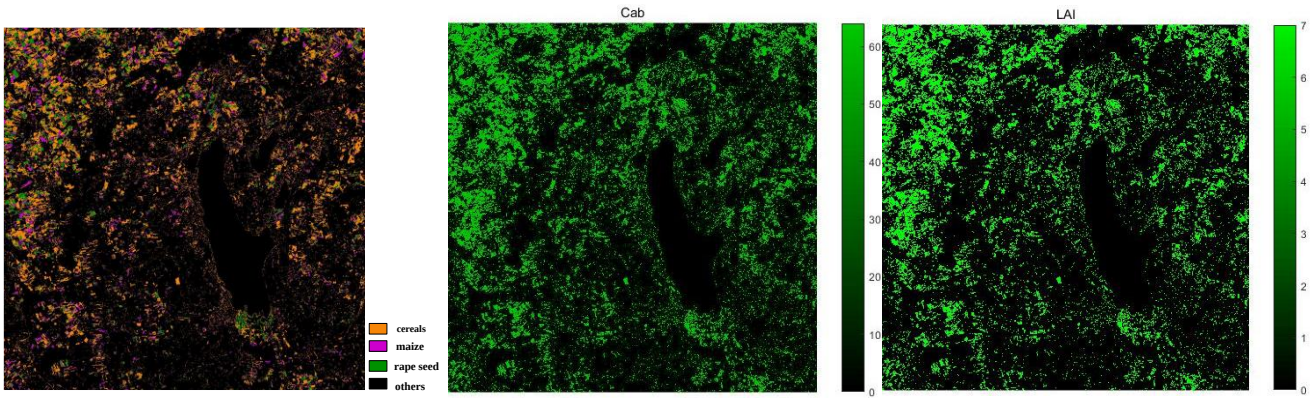


Fig.8. (a) Distribution map of main crops; (b) C_{ab} image map; (c) Leaf area index image map

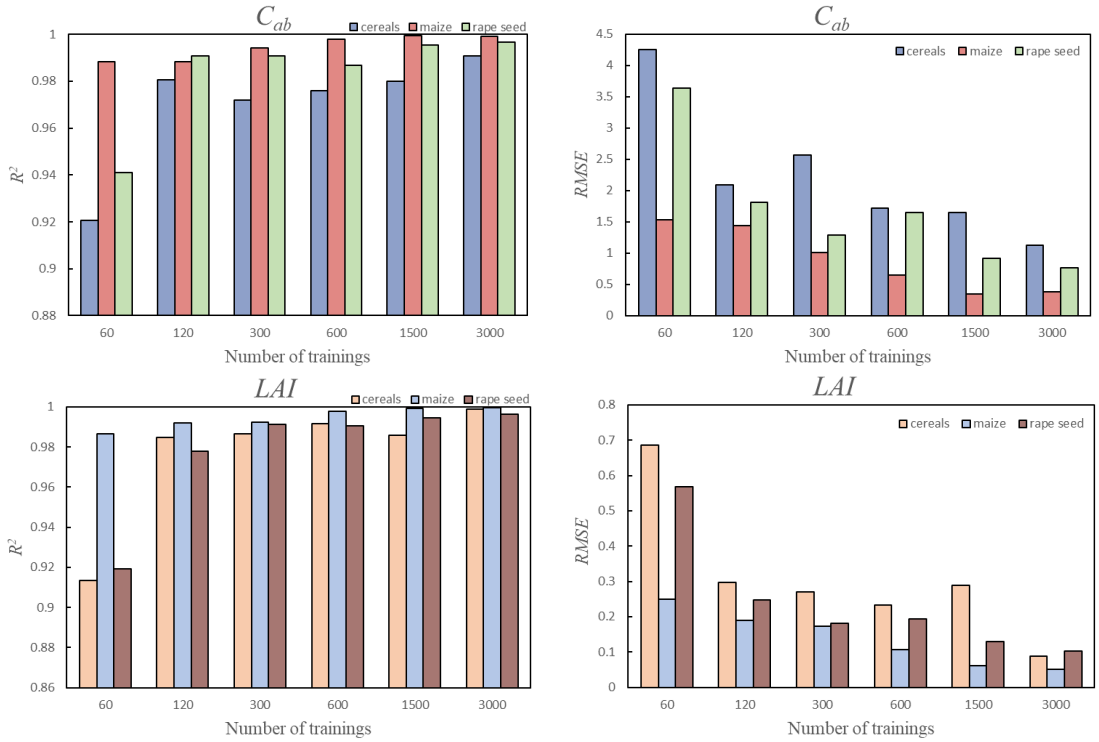


Fig.9. Accuracy maps of the vegetation parameter inversions based on IPROSAIL-Net with the EnMAP data

3.2.2. Experimental results and comparison with EnMAP data

In the comparative analysis, the VGG-16 network was selected for C_{ab} and *LAI* inversions. The settings and sample selection were identical to those used in the IPROSAIL-Net training method. The inversion results and comparisons are presented in TABLE III and Fig. 10.

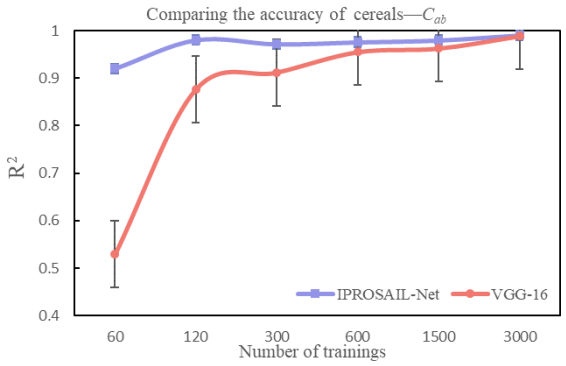
The experimental analysis showed that the vegetation parameter inversion accuracy based on IPROSAIL-Net was equal to or higher than that based on the VGG-16 network. The *RMSE* obtained using IPROSAIL-Net was lower than the *RMSE* obtained with the VGG-16 network inversion. When the number of training iterations was 3000, the R^2 values of cereals, maize, and rapeseed obtained using IPROSAIL-Net were 0.99, the *RMSE* values of C_{ab} were 1.12, 0.38, and 0.76, respectively, and the *RMSE* values of *LAI* were 0.09, 0.05, and 0.10, respectively. The corresponding R^2 obtained using the VGG-16 network were 0.99, the *RMSE* values of C_{ab} were 1.62, 0.86, and 1.31, and the *RMSE* values of *LAI* were 0.20, 0.13, and 0.30, respectively. In summary, the IPROSAIL-Net inversion of C_{ab} and *LAI* using EnMAP data achieved satisfactory results.

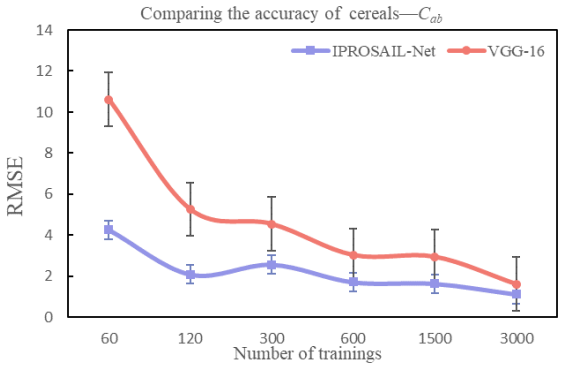
TABLE III

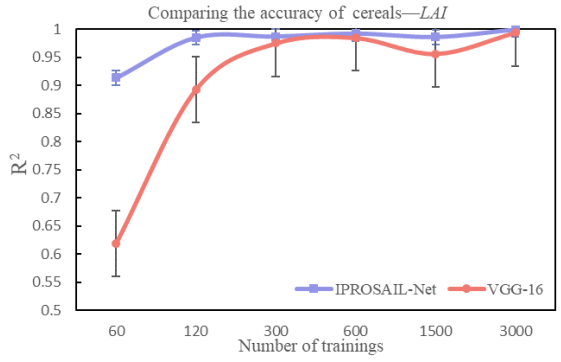
COMPARISON OF CHLOROPHYLL A+B CONTENT (CAB) AND LEAF AREA INDEX (LAI) INVERSION RESULTS WITH THE IPROSAIL-NET AND VGG-16 NETWORKS USING ENMAP DATA

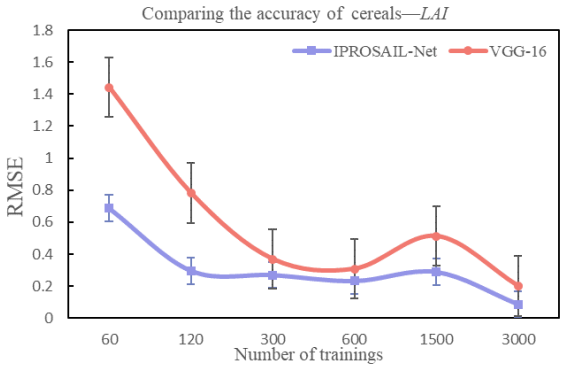
Category	Number of trainings	Category	C_{ab}		*LAI*	
			R^2	*RMSE*	R^2	*RMSE*

Cereals	3000	IPROSAIL-Net	0.99	**1.12**	0.99	**0.09**
		VGG-16	0.99	1.62	0.99	0.20
	1600	IPROSAIL-Net	**0.98**	**1.64**	**0.99**	**0.29**
		VGG-16	0.96	2.96	0.96	0.51
	600	IPROSAIL-Net	**0.98**	**1.71**	**0.99**	**0.23**
		VGG-16	0.96	3.03	0.98	0.31
	300	IPROSAIL-Net	**0.97**	**2.57**	**0.98**	**0.27**
		VGG-16	0.91	4.55	0.97	0.36
	120	IPROSAIL-Net	**0.98**	**2.09**	**0.98**	**0.29**
		VGG-16	0.88	5.26	0.89	0.78
	60	IPROSAIL-Net	**0.92**	**4.25**	**0.91**	**0.68**
		VGG-16	0.52	10.62	0.62	1.44
Maize	3000	IPROSAIL-Net	0.99	**0.38**	0.99	**0.05**
		VGG-16	0.99	0.86	0.99	0.13
	1600	IPROSAIL-Net	0.99	**0.34**	0.99	**0.06**
		VGG-16	0.99	1.03	0.99	0.14
	600	IPROSAIL-Net	0.99	**0.64**	0.99	**0.11**
		VGG-16	0.99	1.12	0.99	0.15
	300	IPROSAIL-Net	0.99	**1.01**	**0.99**	**0.17**
		VGG-16	0.99	1.36	0.96	0.21
	120	IPROSAIL-Net	**0.99**	**1.44**	0.99	**0.19**
		VGG-16	0.96	2.44	0.99	0.37
	60	IPROSAIL-Net	**0.99**	**1.52**	**0.99**	**0.25**
		VGG-16	0.98	1.89	0.90	0.70
Rapeseed	3000	IPROSAIL-Net	0.99	**0.76**	0.99	**0.10**
		VGG-16	0.99	1.31	0.99	0.13
	1600	IPROSAIL-Net	0.99	**0.91**	0.99	**0.13**
		VGG-16	0.99	1.03	0.99	0.15
	600	IPROSAIL-Net	**0.99**	**1.64**	0.99	**0.19**
		VGG-16	0.98	1.82	0.99	0.20
	300	IPROSAIL-Net	0.99	**1.29**	**0.99**	**0.18**
		VGG-16	0.99	1.98	0.98	0.21
	120	IPROSAIL-Net	**0.99**	**1.81**	**0.98**	**0.25**
		VGG-16	0.90	5.25	0.86	0.61
	60	IPROSAIL-Net	**0.94**	**3.61**	**0.92**	**0.57**
		VGG-16	0.93	3.97	0.69	1.05









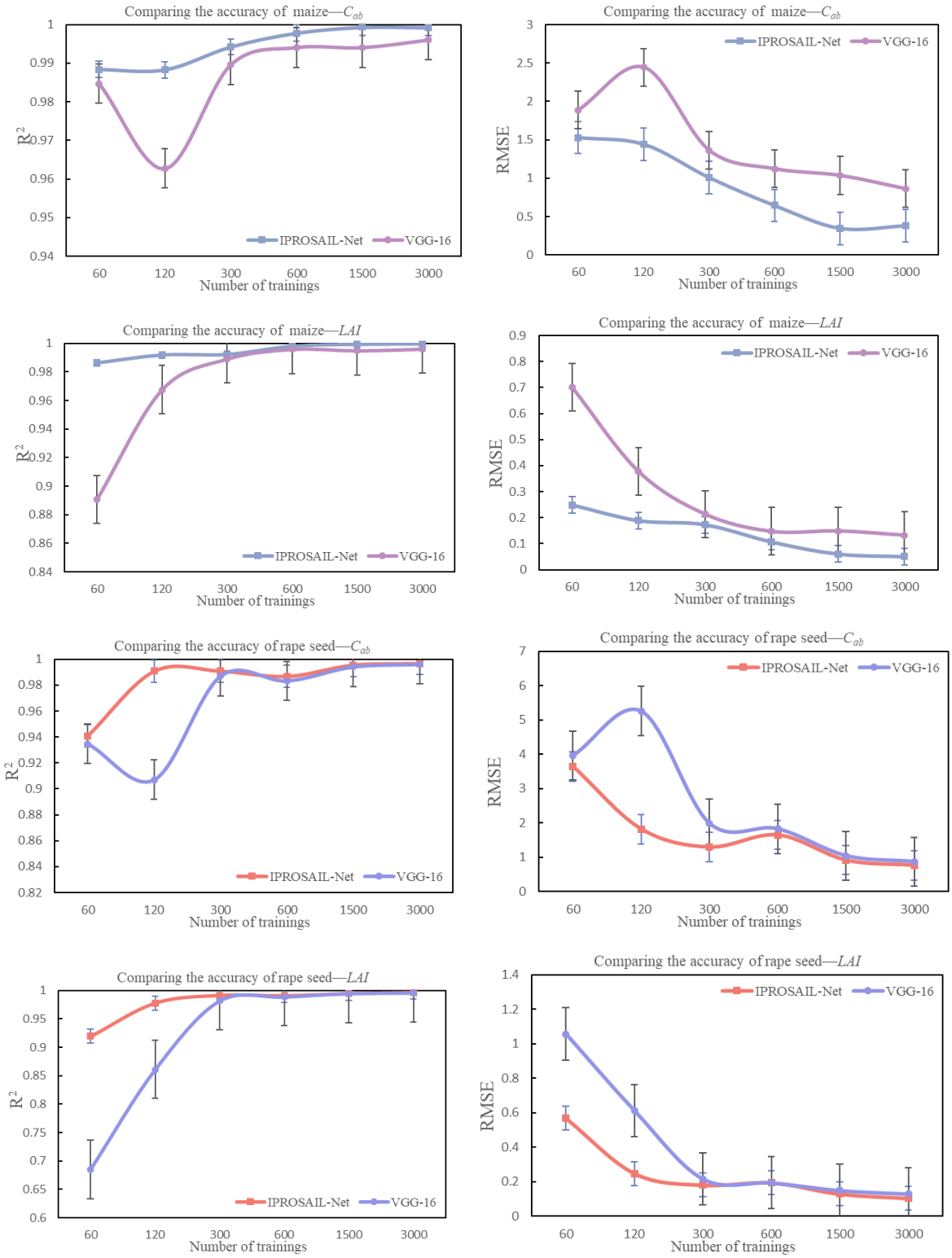


Fig. 10. Vegetation parameters accuracy comparison with EnMAP data

3.3. Submodule training with the IPROSAIL-Net

The IPROSAIL-Net design was divided into modules to verify its rationality. Numerical experimental verification was performed with PROSAIL simulation sample data. IPROSAIL-Net is composed of two branch networks, which use N, C_{ab}, C_w, and C_m and LAI as the output; Para-Net and LAI-Net are used for training and verification, respectively. The PROSAIL model combines the SAIL and PROSPECT models. In this study, ParaNet was divided into two networks, ISAIL-Net and IPROSPECT-Net, for training and verification, respectively. ISAIL-Net uses spectral reflectance as the input, and leaf reflectivity and transmittance as the outputs.

IPROSPECT-Net is a network with leaf reflectivity and transmittance as inputs and leaf parameters C_{ab}, N, C_m, and C_w as outputs.

In this section, the third and fourth modules of the inverse process of the SAIL model are verified as separate subnetwork modules to prove the rationality of their design, followed by verification of the entire subnetworkfied. Because the third network module of the SAIL model inverse process in IPROSAIL-Net has 128 channels, this module should be the input of two channels, namely r_{so} and r_{do}. Therefore, to preserve as much data as possible in multiple channels, designing additional dimensionality reduction adaptation modules to match the positive process is necessary. In this study, a convolution layer with a convolution kernel size of 1×3 and 64 channels was added at the beginning of the subnetwork module, and a convolution layer with a convolution kernel size of 1×3 and 64 channels was added at the end. Layers and 1 fully connected layer. Taking the training sample at 30,000 as an example, the loss function value of the processed subnetwork module on the training and validation sets was lower and gradually decreased, showing a convergence trend. The R^2 values of the five parameters obtained by inversion were all above 0.98, and the *RMSE* values were below 0.11. This demonstrates the rationality of this part of the design.

Similarly, when verifying the fourth module of the inverse process of the SAIL model, additional dimensionality-reducing adaptation modules must be designed to match the positive process. The processing method was identical to that used to verify the third module in the inverse process of the SAIL model. Considering a training sample of 30,000 as an example, the loss function value of the processed subnetwork module on the training and validation sets was lower and gradually decreased, showing a convergence trend. The R^2 values of the five parameters obtained by inversion were all above 0.98, and the *RMSE* values were below 0.11. This demonstrates the rationality of this part of the design.

Next, we verified Para-Net, which uses spectral data as inputs and C_{ab}, N, C_m, and C_w as outputs. The data processing and training methods were the same as those used for IPROSAIL-Net. The training samples were set to 300,000, 60,000, 30,000, 6,000, 3.000, and 1.500. The results are listed in TABLE IV.

TABLE IV
INVERSION OF THE LEAF PARAMETERS BASED ON THE PARA-NET NETWORK

Model	Number of tests	C_{ab}		N		C_m		C_w	
		R^2	*RMSE*	R^2	*RMSE*	R^2	*RMSE*	R^2	*RMSE*
net_{300000}	100000	0.99	0.74	0.99	0.01	0.99	0.0003	0.99	0.0004
net_{60000}	20000	0.99	1.17	0.99	0.02	0.99	0.0004	0.99	0.0006
net_{30000}	10000	0.99	1.37	0.99	0.02	0.99	0.0005	0.99	0.0007
net_{6000}	2000	0.99	1.73	0.98	0.06	0.99	0.0007	0.99	0.001
net_{3000}	1000	0.99	2.84	0.98	0.06	0.99	0.0009	0.98	0.002
net_{1500}	500	0.97	5.03	0.98	0.071	0.98	0.001	0.97	0.002

In the numerical experimental analysis, Para-Net inverted C_{ab}, N, C_m, and C_w with high accuracy for different numbers of samples and the accuracy remained above 0.97. The experimental results demonstrate that the ParaNet network module design is reasonable.

To verify the rationality of the network design further, ParaNet was divided into two networks, ISAIL-Net and IPROSPECT-Net, for training and verification, respectively. First, 50,000 data points were simulated using the PROSAIL model, and the values of spectral reflectance, leaf reflectance, leaf transmittance, and leaf parameters C_{ab}, N, C_m, and C_w were saved. Second, the data were divided into training, verification, and test sets in proportions of 60%, 20%, and 20%, respectively. The corresponding training and validation set samples were then passed to ISAIL-Net and IPROSPECT-Net to train the two networks. The corresponding test samples were then transmitted to a trained network. Finally, the corresponding network inversion values were obtained and the R^2 and *RMSE* values were calculated.

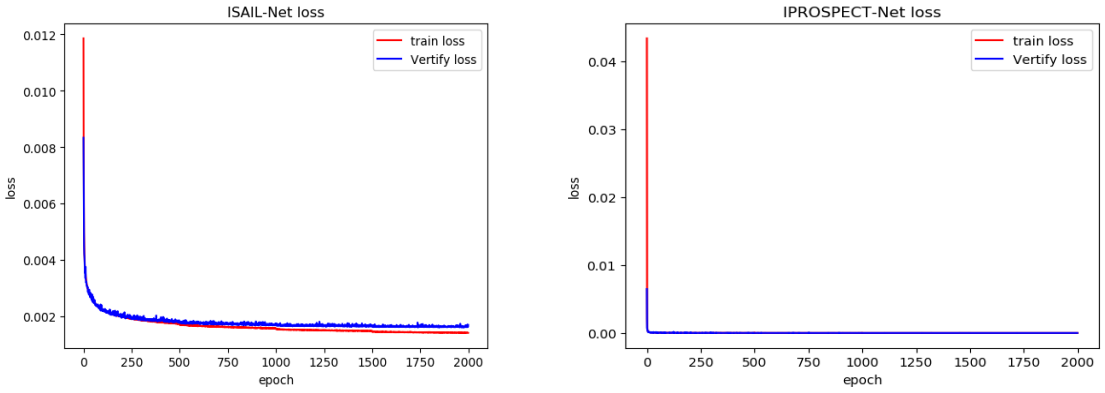
In the process of training ISAIL-Net, the accuracy of the loss function of the training and verification sets reached 10^{-3} before gradually decreasing and converging, as shown in Fig. 11. ISAIL-Net was stable. After training ISAIL-Net, the leaf reflectance and transmittance were obtained by inversion. The calculated leaf reflectance R^2 was 0.9489 and the *RMSE* was 0.0380. The leaf transmittance R^2 was 0.9473 and *RMSE* was 0.0387. ISAIL-Net can clearly invert the leaf reflectance and transmittance with high precision; therefore, the ISAIL-Net design is reasonable. The experimental results further demonstrate that the design of the ISAIL-Net module is reasonable.

In the process of training IPROSPECT-Net, the accuracy of the loss function of the training and verification sets reached 10^{-7} before gradually decreasing and converging, as shown in Fig. 11. After training the IPROSPECT-Net network, C_{ab}, N, C_m and C_w were obtained via inversion. The R^2 values were above 0.99, and the *RMSE* values were 0.053 for 9.3×10^{-4}, 3×10^{-5}, and 2×10^{-5}, respectively. IPROSPECT-Net could invert the four values of the leaf parameters with high precision; therefore, the design of IPROSPECT-Net is reasonable.

LAI-Net used spectral data as the input and *LAI* as the output. The data processing and training methods were identical to those used in IPROSAIL-Net. The training samples were set to 300,000, 60,000, 30,000, 6,000, 3,000, and 1,500. The R^2 values obtained by the inversion were 0.99, 0.99, 0.98, 0.95, 0.95, and 0.92, respectively. The *RMSE* were 0.17, 0.30, 0.38,

0.68, 0.65, and 0.84, respectively. The experimental results further demonstrated that the design of the LAI-Net module is reasonable.

The experimental results show replacing the inverse process of the PROSAIL model with IPROSAIL-Net is reasonable so that vegetation parameter inversion can be performed.



(a) (b)

Fig. 11 Network loss function. (a) ISAIL-Net network loss function; (b) IPROSPECT-Net network loss function

IV. Conclusion

To improve the inversion accuracy of the physical model and neural network mechanism, this study proposes a PROSAIL model inverse process simulation method based on deep learning. The PROSAIL model was first divided into the SAIL and PROSPECT models. Subsequently, based on the physical process and mathematical model, the two models were modularised. Network modules such as the convolutional layer, maximum pooling layer, and fully connected layer were selected to replace the inverse process of each module according to the network principle and finally combined into IPROSAIL-Net. The convolutional, maximum pooling, and fully connected layers reveal the feature extraction of the spectrum and reduce dimensionality. IPROSAIL-Net inverted five values of the vegetation parameters simultaneously, and the rich gradient information in the forward and backward propagation processes stabilised the network combination. Therefore, better vegetation parameter prediction was achieved.

To prove that IPROSAIL-Net can invert vegetation parameters with high precision in different datasets, experiments were carried out using PROSAIL simulation data and EnMAP data. The results showed that vegetation parameters could be inverted with high precision in both datasets. IPROSAIL-Net was then divided into six networks for separate training. The value of the loss function of each network proved that the design of the PROSAIL model was reasonable and that IPROSAIL-Net based on the PROSAIL model could invert vegetation parameters with high precision.

In conclusion, The proposed IPROSAIL-Net network has high accuracy in inverting vegetation parameters using simulated data and EnMAP data. Due to the complexity of the network, its slow training speed, and the limited data we utilize, our goal in future research is to continue optimizing the network for fast and efficient training. And we hope to achieve higher precision vegetation parameter inversion based on small sample datasets and parameter inversion based on multispectral remote sensing data.

Acknowledgments

We thank Prof. Wout Verhoef for providing the singularity calculation process in the SAIL model.

References

[1] Abdelbaki, A., Schlerf, M., Verhoef, W., *et al*. "Introduction of variable correlation for the improved retrieval of crop traits using canopy reflectance model inversion," *Remote sensing*, vol. 11, no. 22, pp. 2681-2701, 2019. DOI: 10.3390/rs11222681.

[2] Abdelmoula, H., Kallel, A., Roujean, J.L., *et al*. "Bayesian inversion technique of olive tree biophysical properties using Sentinel-2 images," *2018 4th International Conference on Advanced Technologies for Signal and Image Processing (ATSIP)*, 2018.

[3] Bahrami, H., Homayouni, S., Safari, A., *et al*. "Deep learning-based estimation of crop biophysical parameters using multi-source and multi-temporal remote sensing observations," *Agronomy*, vol. 11, no. 7, pp. 1363-1384, 2021. DOI: 10.3390/agronomy11071363

[4] Baret, F., Fourty, T.. "Estimation of leaf water content and specific leaf weight from reflectance and transmittance measurements," *Agronomie*, vol. 17, no. 9-10, pp. 455-464, 1997.

[5] Berger, K., Atzberger, C., Danner, M., *et al*. "Evaluation of the PROSAIL model capabilities for future hyperspectral model environments: A review study," *Remote sensing*, vol. 10, no. 1, pp. 85-110, 2018. DOI: 10.3390/rs10010085.

[6] Bousquet, L., Lachérade, S., Jacquemoud, S., *et al*. "Leaf BRDF measurements and model for specular and diffuse components differentiation," *Remote Sensing of Environment*, vol. 98, no. 2-3, pp. 201-211, 2018. DOI: 10.1016/j.rse.2005.07.005.

[7] Chaabouni, S., Kallel, A., Houborg, R.. "Improving retrieval of crop biophysical properties in dryland areas using a multi-scale variational RTM inversion approach," *International Journal of Applied Earth Observation and Geoinformation*, pp. 102220-102233, 2021. DOI: 10.1016/j.jag.2020.102220.

[8] Féret, J.B., François, C., Asner, G.P, *et al*. "PROSPECT-4 and 5: Advances in the leaf optical properties model separating photosynthetic pigments," *Remote sensing of environment*, vol. 112, no. 6, pp. 3030-3043, 2008. DOI: 10.1016/j.rse.2008.02.012.

[9] Féret, J.B., Gitelson, A.A., Noble, S.D. *et al*. "PROSPECT-D: Towards modeling leaf optical properties through a complete lifecycle," *Remote sensing of environment*, vol. 193, pp. 204-215, 2017.

[10] Houborg, R., Soegaard, H., Boegh, E.. "Combining vegetation index and model inversion methods for the extraction of key vegetation biophysical parameters using Terra and Aqua MODIS reflectance data," *Remote*

sensing of environment, vol. 106, no. 1, pp. 39-58, 2007.
[11] H. Yang, X. Yang, M. Heskel, "Seasonal variations of leaf and canopy properties tracked by ground based NDVI imagery in a temperate forest," *Scientific reports*, vol. 7, no. 1, pp. 1267-1276, 2017. DOI:10.1038/s41598-017-01260-y.
[12] Jacquemoud, S., Baret, F.. "PROSPECT: A model of leaf optical properties spectra," *Remote sensing of environment*, vol. 34, no. 2, pp. 75-91, 1990.
[13] Jacquemoud, S., Baret, F., Andrieu, B., *et al*. "Extraction of vegetation biophysical parameters by inversion of the PROSPECT + SAIL models on sugar beet canopy reflectance data. Application to TM and AVIRIS sensors," *Remote sensing of environment*, vol. 52, no. 3, pp. 163-172, 1995.
[14] Jacquemoud, S., Ustin, S.L., Verdebout, J., *et al*. "Estimating leaf biochemistry using the PROSPECT leaf optical properties model," *Remote sensing of environment*, vol. 56, no. 3, pp. 194-202, 1996.
[15] Jacquemoud, S., Verhoef, W., Baret, F., *et al*. "PROSPECT+ SAIL models: A review of use for vegetation characterization," *Remote sensing of environment*, vol. 113, pp. S56-S66, 2009.
[16] Jiří, T., Jan, M., Petr, L.. "Prototyping a Generic Algorithm for Crop Parameter Retrieval across the Season Using Radiative Transfer Model Inversion and Sentinel-2 Satellite Observations," *Remote Sensing*, vol. 13, no. 18, pp. 3569-3597, 2021. DOI: 10.3390/rs13183659.
[17] Kennedy, B.E., King, D.J., Duffe, J.. "Retrieval of arctic vegetation biophysical and biochemical properties from CHRIS/PROBA multi-angle imagery using empirical and physical Modelling," *Remote sensing*, vol. 13, no. 9, pp. 1830-1860, 2021. DOI: 10.3390/rs13091830.
[18] Makhloufi, A., Kallel, A., Chaker, R., *et al*. "Retrieval of olive tree biophysical properties from Sentinel-2 time series based on physical modelling and machine learning technique," *International Journal of Remote Sensing*, vol. 42, no. 22, pp. 8542-8571, 2021.
[19] Marandi, M., Parida, B.R., Ghosh, S.. "Retrieving vegetation biophysical parameters and GPP using satellite-driven LUE model in a National Park," *Environment, Development and Sustainability*, pp. 1-21, 2021.
[20] Meroni, M., Colombo, R., Panigada, C.. "Inversion of a radiative transfer model with hyperspectral observations for LAI mapping in poplar plantations," *Remote sensing of environment*, vol. 92, no. 2, pp. 195-206, 2004.
[21] Mridha, N., Sahoo, R.N., Sehgal, V.K. "Comparative evaluation of inversion approaches of the radiative transfer model for estimation of crop biophysical parameters," *International Agrophysics*, vol. 29, no. 2, pp. 201-212, 2015. DOI: 10.1515/intag-2015-0019.
[22] NC de Sa, M Baratchi, LT Hauser, *et al*. "Exploring the impact of noise on hybrid Inversionof PROSAIL RTM on Sentinel-2 data," *Remote Sensing*, vol. 13, no. 4, pp. 648-667, 2021. DOI: 10.3390/rs13040648.
[23] Parida, B.R., Kumari, A.. "Mapping and modeling mangrove biophysical and biochemical parameters using Sentinel-2A satellite data in Bhitarkanika National Park, Odisha," *Modeling Earth Systems and Environment*, vol. 7, pp. 2463-2474, 2021.
[24] Pastor-Guzman, J., Atkinson, P.M., Dash, J., *et al*. "Spatiotemporal variation in mangrove chlorophyll concentration using Landsat 8," *Remote sensing*, vol. 7, no. 11, pp. 14530–14558, 2015. DOI: 10.3390/rs71114530.
[25] P. Yang, W. Verhoef, E. Prikaziuk., *et al*. "Improved retrieval of land surface biophysical variables from time series of Sentinel-3 OLCI TOA spectral observations by considering the temporal autocorrelation of surface and atmospheric properties," *Remote sensing of environment*, vol. 256, pp. 112328–112344, 2021. DOI: 10.1016/j.rse.2021.112328.
[26] Sanjiv, K., Sinha Padadra, H., Dasgupta, A., *et al*. "Estimation of leaf area index using PROSAIL based LUT inversion, MLRA-GPR and empirical models: Case study of tropical deciduous forest plantation, North India," *International Journal of Applied Earth Observation and Geoinformation*, vol. 86, pp. 102027–102036, 2020. DOI: 10.1016/j.jag.2019.102027.
[27] Shanqin, W., Wenhan, G.. "A TPE based inversion of PROSAIL for estimateng canopy biophysical and biochemical variables of oilseed rap," *Computers and Electronics in Agriculture*, vol. 152, pp. 350-362, 2018.
[28] Simonyan, K., Zisserman, A.. "Very deep convolutional networks for large-scale image recognition," arXiv Preprint arXiv:1409.1556. 2014.
[29] W. Verhoef.. "Light scattering by leaf layers with application to canopy reflectance modeling: The SAIL model," *Remote sensing of environment*, vol. 16, no. 2, pp. 125-141, 1984.
[30] W. Verhoef.. "Earth Observation Modeling Based on Layer Scattering Matrices," *Remote sensing of environment*, vol. 17, no. 2, pp. 165-178, 1985.
[31] W. Verhoef.. "Theory of Radiative Transfer Models Applied in Optical Remote Sensing of Vegetation Canopies," *Wageningen University and Research*, 1998.
[32] W. Verhoef, H. Bach. "Simulation of hyperspectral and directional radiance images using coupled biophysical and atmospheric radiative transfer models," *Remote sensing of environment*, vol. 87, no. 1, pp. 23-41, 2003.
[33] W. Verhoef, L. Jia, Q. Xiao, *et al*. "Unified optical-thermal four-stream radiative transfer theory for homogeneous vegetation canopies," *IEEE Transactions on geoscience and remote sensing*, vol. 45, no. 6, pp. 1808-1822, 2007. DOI: r 10.1109/TGRS.2007.895844.
[34] J. Verrelst, Z. Malenovský, C. Van der Tol, *et al*. "Quantifying vegetation biophysical variables from imaging spectroscopy data: A review on retrieval methods," *Surveys in Geophysics*, vol. 40, pp. 589-629, 2019. DOI: 10.1007/s10712-018-9478-y.
[35] J. Wu, K. Guan, M. Hayek, *et al*. "Partitioning controls on Amazon Forest photosynthesis between environmental and biotic factors at hourly to interannual timescales," *Global Change Biology*, vol. 23, no. 3, pp. 1240-1257, 2017.
[36] Y. Wu, S. Giri, Z. Qiu. "Understanding the spatial distribution of hydrologic sensitive areas in the landscape using soil topographic index approach," *International Soil and Water Conservation Research*, vol. 4, no. 4, pp. 278–283, 2016. DOI: 10.1016/j.iswcr.2016.10.002.
[37] Q. Xie, J. Dash, A. Huete, *et al*. "Retrieval of crop biophysical parameters from Sentinel-2 remote sensing imagery," *International Journal of Applied Earth Observation and Geoinformation*, vol. 80, pp. 187-195, 2019.
[38] X. Xu, J. Lu, N. Zhang, *et al*. "Inversion of rice canopy chlorophyll content and leaf area index based on coupling of radiative transfer and Bayesian network models," *ISPRS Journal of Photogrammetry and Remote Sensing*, vol. 150, pp. 185-196, 2019.
[39] L. Annala, E. Honkavaara, S. Tuominen, *et al*. "Chlorophyll Concentration Retrieval by Training Convolutional Neural Network for Stochastic Model of Leaf Optical Properties (SLOP) Inversion," *Remote Sensing*, vol. 12, no. 2, pp. 283-304, 2020.



Yunli Han received a B.S. degree in information and computing science from Qilu University of Technology, Shandong, China, in 2017, and a M.S. degree in mathematics of computation from Capital Normal University, Beijing, China, in 2020. Her research interests include research and application in vegetation remote sensing.



Yingying Dong received a B.S. degree in information and computation science from Shandong Normal University, Shandong, China, in 2006, a M.S. degree in mathematics of computation from Capital Normal University, Beijing, China, in 2009, and a Ph.D. degree in agricultural remote sensing and information technology from Zhejiang University, Zhejiang, China, in 2013. Her research interests include research and application in vegetation remote sensing.



Yining Zhu received a B.S. degree in information and scientific computing from the Beijing Information and Technology Institute in 2006 and M. S. and Ph.D. degrees in mathematics and information technology from Capital Normal University, Beijing, China, in 2009 and 2012, respectively. He was a Postdoc at the Peking University, Beijing, China, from 2013 to 2014. He is an associate professor at the School of Mathematical Science, Capital Normal University. His current research interests include image reconstruction, deep-learning-based artefact correction, and image processing.



Wenjiang Huang received a Ph.D. in cartography and GIS from Beijing Normal University, Beijing, China, in 2005. He is a Professor with the Key Laboratory of Digital Earth Science, Aerospace Information Research Institute, Chinese Academy of Sciences, Beijing, China. His research interests include quantitative remote-sensing and vegetation applications.